Submitted to Science and Technology for the Built Environment

Heat Transfer and Pressure Drop of R1123/R32 (40/60 mass%) Flow in Horizontal Microfin Tubes during Condensation and Evaporation

Chieko Kondou

ABSTRACT

In this study, the heat transfer coefficient (HTC) and pressure drop of the new low global warming potential refrigerant mixture R1123/R32 (40/60 mass%) in a 6.0 mm OD horizontal microfin tube during condensation at 40 °C and evaporation at 10 °C are experimentally quantified. The data are then compared to the component R32. Both the condensation HTC and pressure drop of R1123/R32 (40/60 mass%) are somewhat lower than those of R32. Similarly, the pressure drop of R1123/R32 during the evaporation process at 10 °C is somewhat lower than that of R32. However, the evaporation HTC is comparable to that of R32. The lower surface tension of R1123/R32 can enhance the nucleate boiling and compensate the heat transfer degradation due to the volatility difference.

Introduction

For mitigation of global warming, a phase-down schedule of the production and the consumption amount of HFCs (Hydro Fluoro Carbons) and Hydro Chloro Fluoro Carbons (HCFCs) were specifically declared in the Kigali amendment (Heath, 2017) of the Montreal protocol. According to this schedule, by 2036, developed countries should reduce their equivalent amount of CO_2 by 85% from the baseline period of 2011 to 2013. Under these circumstances, low global warming potential (GWP) refrigerants have been attracting the attention of air conditioner and refrigerator manufacturers worldwide. The current commercial focus is mostly on Hydro Fluoro Olefins (HFOs) exhibiting a GWP of less than 1, with the acceptance of mild flammability. HFO-1123 (hereafter designated as R1123 for simplicity) is one example. Although the use of R1123 alone causes the risk of a disproportionation reaction under very high pressure and temperature conditions, this substance has potentially beneficial thermophysical properties as a mixture component coupled with R32. A binary mixture, R1123/R32, is anticipated to be a new candidate R410A alternative used in stationary air conditioning systems. Nevertheless, the characteristics of the heat transfer and pressure drop of these refrigerants have not yet been clarified. As described in many previous studies (e.g., Hui and Thome, 1984; Jung and Radermacher, 1993; Niederküger and Steiner, 1994), volatility differences result in a severe degradation of the heat transfer coefficient (HTC). Therefore, to understand the transport phenomenon of these binary mixtures, the HTC and pressure gradient during the condensation and evaporation process in a horizontal microfin tube are experimentally investigated in this study. Experimental data on R1123/R32 at a composition of 40/60 mass% are compared to R32 alone and to the predicted results based on the correlations proposed for other binary mixtures.

Experimental method

Test loop

Fig. 1 (a) shows a vapor compression cycle facilitating the measurement of the HTC and pressure drop. The HTC and pressure drop are measured in the condensation and evaporation test sections. To determine the bulk enthalpies of superheated vapor, the bulk mean temperature and pressure are measured in mixing chambers placed at the inlet of the precooler and at the outlet of the superheater. Additionally, the circulation composition is measured by sampling approximately 1 cc of subcooled liquid at the outlet of the liquid reservoir just after the data are recorded. The sampled liquid is completely vaporized in a sampling vessel, and then assayed using a thermal conductivity detector gas chromatograph. The refrigerant state is evaluated under the circulation composition. Based on the bulk enthalpies of the superheated vapor, the enthalpies in the test sections are calculated by considering the enthalpy changes in the precooler, superheater, and the test sections obtained from the water side heat balance.

[Fig. 1 Experimental apparatus. (a) test loop (b) structure of the test section (evaporator)]

Fig. 1 (b) illustrates the structure of the test sections. A horizontally placed test microfin tube is surrounded by two water jackets and connected to the pressure ports for measuring the heat transfer rates over the 414-mm length and pressure drops at 554-mm intervals. At each subsection (i.e., the water jacket), eight thermocouples were embedded outside of the tube wall. The internal tube surface temperature, T_{wi}, is obtained from the measured outer tube temperature considering the one-dimensional heat conduction of the tube wall.

$$T_{wi} = \left(T_{wo,top} + T_{wo,bottom} + T_{wo,right} + T_{wo,left}\right)/4 - \left[Q_{H2O\,TS}/\left(2\pi\Delta Z\lambda_{tube}\right)\right]\ln\left(d_o/d_{eq}\right) \quad (1)$$

The representative refrigerant temperature of each subsection, $T_{r\,TS}$, is defined as the arithmetic mean of the inlet and outlet calculated from the obtained enthalpies and pressures by assuming thermodynamic equilibrium with the optimized equation of state (EOS) associated with REFPROP 9.1 (Lemmon et al., 2013).

$$T_{r\,TS} = \left(T_{r\,TS,i} + T_{r\,TS,o}\right)/2 \quad (2)$$

$$T_{r\,TS,i} = f_{EOS}\left(h_{r\,TS,i}, P_{r\,TS,i}, X_{R1123}\right), \quad T_{r\,TS,o} = f_{EOS}\left(h_{r\,TS,o}, P_{r\,TS,o}, X_{R1123}\right) \quad (3)$$

Similarly, the representative vapor quality of each subsection, x, is calculated as follows:

$$x_{TS} = \left(x_{TS,i} + x_{TS,o}\right)/2 \quad (4)$$

$$x_{TS,i} = f_{EOS}\left(h_{r\,TS,i}, P_{r\,TS,i}, X_{R1123}\right), \quad x_{TS,o} = f_{EOS}\left(h_{r\,TS,o}, P_{r\,TS,o}, X_{R1123}\right) \quad (5)$$

Based on the actual heat transfer area, the heat flux, q, and the HTC, α, are defined as follows:

$$\alpha_{TS1} = q_{TS1}/\left(T_{r\,TS1} - T_{wi}\right) \quad (6)$$

$$q_{TS1} = Q_{H2O\,TS1}/\left(\pi d_{eq}\eta_A \Delta Z\right) \quad (7)$$

A deviation of within 1 kW m^{-2} of the targeted average heat flux was allowed to adjust for the test conditions, except for the dryout condition. An experiment is carried out at a pressure corresponding to the average of the bubble and dew temperatures equal to 40 °C for the condensation tests and 10 °C for evaporation tests. The uncertainty in each measurement parameter is listed in Table 1. From those uncertainty data, the propagated uncertainty in HTC and pressure drop are calculated.

[Table 1 Instrumentation and measurement uncertainty.]

Test microfin tube

Fig. 2 shows microscopic images of the cross-sectional area of the test microfin tube. The dimensions are specified in Table 2. The equivalent inner diameter, d_{eq}, is the inner diameter of a smooth tube that envelops an equal internal-free-flow-volume. The surface enlargement, η_A, is the ratio of the actual heat transfer area to that of the equivalent smooth tube. In this study, the mass velocity is defined with a cross-sectional free flow area considering the helix angle. The HTC and heat flux also are defined using the actual heat transfer area.

[Fig. 2 Sectional view of the tested microfin tube.]

[Table 2 Dimensions of the test microfin tube.]

Test refrigerants

In this experiment, R32 and a binary mixture R1123/R32 are examined. The test refrigerant R1123/R32 (40/60 mass%) was supplied by AGC Inc. The purity and nominal composition was more than 99.998 mol% and 39.3/60.7 mass%, respectively, as the assay result. Table 3 lists the basic information and thermophysical properties of R32 and R1123/R32 (40/60 mass%) evaluated at an average saturation temperatures of 40 °C and 10 °C. By fitting the measured data, the EOS was proposed for R1123 (Higashi and Akasaka, 2016). With this EOS, the thermodynamic properties of mixture R1123/R32 (40/60 mass%) is calculated with a mixture model (Kunz and Wagner, 2012) without excess energy by the mutual interaction that is designated as KW0 model in REFPROP 9.1 (Lemmon et al., 2013). Fig. 3 shows the calculated phase equilibrium compared to that of R32/R1234ze(E) (60/40 mass%), which is considered other potential alternatives of R410A. The temperature glide and the mole fraction difference between liquid and vapor of R1123/R32 (40/60 mass%) are significantly smaller than those of R32/R1234ze(E) (60/40 mass%). The theoretical cooling capacity, which is a product of the vapor density and latent heat, of R1123/R32 (40/60 mass%) is 10.0 MJ m^{-3}. That is 11 % larger than that of R32, which is 9.0 MJ m^{-3}. Therefore, the drop-in of R1123/R32 (40/60 mass%) can potentially achieve the same or higher cooling performance if the irreversible losses by heat transfer and pressure drop were not increased. The surface tension is calculated as 3.60 and 8.27 mNm^{-1} by an empirical correlation proposed on the basis of the measured data (Kondou et al., 2018).

$$\sigma = \sigma_0 \left[1-(T+273.15)/(T_{\text{crit}}+273.15)\right]^c \qquad [\text{mNm}^{-1}]$$

where, $\sigma_0 = \sigma_{0,R1123}\bar{\theta}_{R1123} + \sigma_{0,R32}\bar{\theta}_{R32} - 4.1\cdot\bar{\theta}_{R1123}\bar{\theta}_{R32}$

$$\bar{\theta}_{R1123} = \frac{\bar{X}_{R1123}V_{\text{crit, R1123}}^{2/3}}{\bar{X}_{R32}V_{\text{crit, R32}}^{2/3} + \bar{X}_{R1123}V_{\text{crit, R1123}}^{2/3}}, \quad \bar{\theta}_{R32} = 1-\bar{\theta}_{R1123} \tag{8}$$

$$c = c_{R32} + (c_{R1123} - c_{R32})\bar{\theta}_{R1123},$$

and $\begin{cases}\sigma_{0,R1123} = 61.02, & c_{R1123} = 1.30 \\ \sigma_{0,R32} = 71.47, & c_{R32} = 1.246\end{cases}$ (Murelo et al., 2014)

The transport properties, liquid thermal conductivity and viscosity, are estimated by the extended corresponding states model (Klein et al., 1997; Huber et al., 1992) associated with REFPROP 9.1 (Lemmon et al., 2013). Because the mixing model and the transport property correlations are not yet well established for the tested refrigerant, it should be noted that the error in measured and predicted results might be unexpectedly large.

[Table 3 Basic information and thermophysical properties of the tested refrigerants.]

[Fig. 3 Phase equilibria of R1123/R32 and other R410A alternative candidate R32/R1234ze(E) at an average saturation temperature of 10 °C.]

Check for refrigerant saturation temperature

The saturation temperature of the mixtures depends on the composition, pressure, and vapor quality. This means the temperature can include a larger uncertainty. Thus, the saturation temperature should be carefully checked for the new mixture, the property data of which have not been adequately reported.

For a validation of the method determining the saturation temperature, Figs. 4 (a) (b) plot the deviation in the measured bulk mean refrigerant temperature calculated using the KW0 model (default Kuntz-Wagner model) provided by REFRPOP 9.1. As for comparison, Figs. 4(c) (d) plot the deviation in saturation temperature of R32. The bulk mean refrigerant temperatures are measured in mixing chambers placed at the test section inlet and outlet with an uncertainty of approximately ±0.05 K. The calculated refrigerant temperature corresponds to the saturation temperature at the measured local pressure and the obtained enthalpy. The uncertainty in the calculated temperature is typically ±0.085 K. As shown in Fig. 4 (a), the measured temperature negatively deviates from the calculation at a saturation temperature of 40 °C. The same tendency is shown for both the test section inlet and outlet. The average deviation is consistently -0.17 K. It appears to be that the mixing model, which has not yet been optimized for R1123/R32, results in a slightly higher saturation temperature than the true value. Based on this, an offset of -0.17 K in the saturation temperature was chosen for the condensation test. Fig. 4 (b) shows the results at an average saturation temperature of 10 °C. The measured refrigerant temperature randomly deviates because of the larger fluctuation in the measured pressure during the evaporation test. Nevertheless, no obvious or systematic deviation, or bias, was shown, and most of the data agree with the calculated temperature within the uncertainty. Fortunately, the default KW0 model gives almost the exact temperature at 10 °C. Therefore, in this study, for the evaporation test, the saturation temperature is simply calculated using the KW0 model without an offset.

[Fig. 4 Comparison on refrigerant saturation temperature between the measured and calculated with KW0 model. (a) for condensation test (b) for evaporation test (c) for condensation test (d) for evaporation test]

Results and discussion

HTC and Pressure Drop of R1123/R32 (40/60 mass%)

Figs. 5(a) and 5(b) show the condensation HTC and pressure drop, respectively, as a function of the liquid quality, which were experimentally quantified for R1123/R32 (40/60 mass%) at a heat flux of 10 kWm^{-2} and a pressure of 2.84 MPa corresponding to an average saturation temperature of 40 °C, and a mass velocity of 200 to 400 kg $m^{-2}s^{-1}$. The bars appended to the symbols show the propagated measurement uncertainty of 95% confidence level (Taylor, 1997) in the HTC or the pressure drop in the vertical direction, and the vapor quality over a subsection in the horizontal direction. Because the uncertainty in pressure drop is typically ±0.28 kPa m^{-1}, the vertical bars are smaller than the plotted symbols. The lines indicate the predicted HTC and pressured drop based on the correlations of Yonemoto-Koyama (2007), and Silver (1942) and Bell-Ghaly (1973) taking into account the heat transfer degradation owing to the volatility difference for HTC, and based on Baba (2013) for the pressure drop, *DP*/*DZ*. The correction method of Silver (1942) and Bell-Ghaly (1973) were proposed for HFC mixtures and later validated with other HFO/HFC mixtures, R32/R1234ze(E) and R744/R32/R1234ze(E) by Kondou et al. (2015). The correlation of Baba (1973) is empirically obtained with data of R134a, R32, R1234ze(E), R32/R1234ze(E) and R410A flows during condensation and evaporation. The variation in measured HTC agrees well with the predicted value except at liquid qualities of less than 0.2, where the uncertainty becomes notably large. In addition, the measured pressure drop agrees with the prediction within the measurement uncertainty.

[Fig. 5 R1123/R32 (40/60 mass%) condensation test results at various mass velocities. (a) heat transfer coefficient (b) pressure drop]

Figs. 6(a) and 6(b) show the evaporation HTC and the pressure drop, respectively, as a function of vapor quality at a pressure of 1.31 MPa corresponding to an average saturation temperature of 10 °C, and a mass velocity of 200 to 400 kg $m^{-2}s^{-1}$. The HTC increases with an increase in vapor quality, and then sharply decreases under a vapor quality of approximately 0.8, which indicates a typical dryout occurrence in a horizontal tube. Similarly, the pressure drop increases with the increase in vapor quality of up to 0.9 and then gradually decreases or plateaus. The measured data are compared to the existing predictions, which are shown with the solid lines in Figs. 6(a) and 6(b). For HTC, the correlation of Kondou et al. (2013) proposed for R32/R1234ze(E) and Yoshida et al. (2000) proposed for the HTC in a dryout region of other HFC single components is selected. This correlation predicting onset-dryout is established based on the data of HFC refrigerant evaporation HTC in a microfin tube with an equivalent inner diameter of 6.38 mm. For the pressure drop, the correlation of Baba (2013) proposed for R32/R1234ze(E) is selected. Although the selected correlation underestimates the HTC at vapor qualities of 0.6 to 0.9, a reasonable prediction is given at lower vapor qualities and in the dryout region at a mass velocity of 200, 300, and 400 kg $m^{-2}s^{-1}$. On the other hand, the correlation of Baba provides a precise prediction in the entire measured region. Fig. 6 (c) shows the evaporation HTC at a mass velocity of 200 kgm^{-2} and various heat fluxes. Before the onset dryout, the HTC at a heat flux of 5 kWm^{-2} is somewhat lower than that at 10 kWm^{-2} probably because of the less nucleate boiling contribution. Then, the onset dryout at 5 kWm^{-2} appears at higher vapor quality than that at 10

kWm^{-2}. This is common behavior among the refrigerants having similar normal boiling point. However, the HTC at 15 kWm^{-2} is almost comparable to 10 kWm^{-2} and the onset dryout appears at notably lower vapor quality than 10 kWm^{-2} and that predicted by the correlation. This could be the combined consequence of the lower vapor velocity (higher vapor density) and the mass transfer resistance by zeotropicity.

[Fig. 6 R1123/R32 (40/60 mass%) evaporation test results at various mass velocities and heat fluxes. (a) heat transfer coefficient at various mass velocities (b) pressure drop at various mass velocities (c) heat transfer coefficient at various heat fluxes]

Comparison between R1123/R32 (40/60 mass%) and R32 alone

Figs. 7 and 8 compare the condensation and evaporation HTC and the pressure drop between R1123/R32 (40/60 mass%) and the component R32 at average temperatures of 40 °C and 10 °C, a mass velocity of 200 kg $m^{-2}s^{-1}$, and a heat flux of 10 kWm^{-2}.

[Fig. 7 Comparison between R1123/R32(40/60 mass%) and R32 at 40 °C during condensation. (a) heat transfer coefficient (b) pressure drop]

The condensation HTC of R1123/R32 (40/60 mass%) is somewhat lower than that of the component R32 alone. This can be explained through the higher liquid thermal conductivity and lower vapor density of R32, as specified in Table 3. At a given mass velocity, the lower vapor density indicates a higher vapor velocity, and a greater convective contribution can be expected in the condensation heat transfer, which is also helped by the higher thermal conductivity. Instead, the pressure drop of R32 becomes somewhat higher than that of R1123/R32 (40/60 mass%). The heat transfer degradation caused by the mass transfer resistance is not severe for R1123/R32 (40/60 mass%). These characteristics seem to be well explained based on the predictions plotted by the solid lines.

In Fig. 8, the calculated HTC by a correlation proposed by Thome et al. (1997) for single components of HFCs is plotted for R32. This is because the correlation of Kondou et al. (2013) results an error at mass fractions of 0/100 mass% and 100/0 mass%. The continuous calculation results from 1/99 mass% to 99/1 mass% are shown in Fig. 9. The evaporation HTC of R1123/R32 (40/60 mass%) is almost comparable to that of R32 alone. One reason for this is the much lower surface tension of R1123/R32 (40/60 mass%) than that of R32, as shown in Table 3. This can enhance the nucleate boiling contribution in the evaporation HTC. The HTC predicted using the thermodynamic properties and the estimated transport properties still agree satisfactorily with the measured data for both refrigerants. At present, the effects of the transport properties, e.g., the thermal conductivity, are unclear because of a lack in precise measurement data. The pressure drop of R1123/R32 (40/60 mass%) is clearly lower than that of R32 alone owing to the slower vapor velocity from the higher vapor density. The correlation of Baba (2013) shows a high degree of overlap with the measured pressure drop data and reasonably reflects the effects of the vapor velocity. Further discussions, such as the viscosity effect of the pressure drop, will be available when the transport property measurement data are reported for this mixture.

[Fig. 8 Comparison between R1123/R32(40/60 mass%) and R32 at 10 °C during evaporation.
(a) heat transfer coefficient (b) pressure drop]

Fig. 9 shows the change in evaporation HTC of R1123/R32 (40/60 mass%) and other binary mixture R32/R1234ze(E) against the R32 mass fraction, i.e., circulation composition. Probably the HTC of R1123 alone, which is operated at higher reduced pressure, is higher than R32 likely because of the lower surface tension and smaller latent heat. For instance, it was well documented that carbon dioxide operated at pressures very close to the critical point is very volatile and exhibits considerably higher HTC than that of other refrigerants such as R134a and R410A. R1123 alone would show the similar evaporation heat transfer behavior. The HTC of a binary mixture is very often decreased by the mass transfer resistance which is caused by the concentration boundary at the liquid-vapor interface and excess sensible heat exchange caused by the temperature glide. That is the reason why the HTC of R32/R1234ze(E) is lower than that of R1234ze(E) and reaches a minimum at the R32 mass fraction of approximately 0.2, where the mass fraction difference of vapor and liquid and the temperature glide is maximized. The zeotropicity of R1123/R32 is obviously smaller than the other mixture R32/R1234ze(E), as shown in Fig. 3. The heat transfer degradation due to the mass transfer resistance seems notably small for R1123/R32, according to the prediction given with the estimated properties.

[Fig. 9 Estimated change in HTC of binary mixtures against R32 mass fraction.]

Conclusions

The HTC and pressure drop in a horizontal microfin tube with an outer diameter of 6.0 mm have been experimentally qualified for a newly nominated low GWP refrigerant mixture, R1123/R32, at a nominal composition of 40/60 mass%, and an average saturation temperature of 40 °C in the condensation test and 10 °C in the evaporation test. The condensation HTC at 40 °C was somewhat lower than that of R32. The evaporation HTC of R1123/R32 (40/60 mass%) was almost comparable to that of R32 alone, which suggests that the heat transfer degradation by the mass transfer resistance is notably small compared to other recently proposed mixtures. In the evaporation heat transfer, the smaller surface tension of R1123/R32 enhances the nucleate boiling and compensates the mass transfer resistance. On the other hand, the pressure drop of R1123/R32 (40/60 mass%) during both condensation and evaporation was obviously lower than that of R32 because of the higher vapor density. At the present stage, the mixing model is still being developed, and transport property measurements are ongoing for R1123/R32. The more specific contribution of the model will be revealed when it becomes better established. However, it should be noted that the above comparison was made at the same mass velocity. The systems using those refrigerants can be operated under a given compressor displacement, if drop-in, or a given rating cooling/heating capacity. Thus R1123/R32 can be used in the systems at higher mass velocities by approximately 20% to 35% than R32. This can mitigate lower HTC but can cancel the lower pressure drop of R1123/R32.

Acknowledgments

The sample refrigerants were kindly donated by AGC Inc., Japan. The test microfin tube was kindly provided by Kobelco and Materials Copper Tube, Ltd. This study was financially supported by the New Energy and Industrial Technology Development Organization (NEDO). The authors thankfully acknowledge their support.

References

Baba, D., 2013. An experimental study on condensation and evaporation of low GWP refrigerants in microfin tubes. Doctor thesis, Kyushu University, Inter disciplinary Graduate School of Engineering Sciences.

Bell, K.J., and M.A. Ghaly. 1973. An approximate generalized design method for multicomponent/partial condenser. *AIChE Symposium Series* 69:72–9.

Heath, E., 2017. Amendment to the Montreal Protocol on Substances that Deplete the Ozone Layer (Kigali Amendment). *International Legal Materials*, 56(1), 193-205.

Higashi, Y., Akasaka, R., 2016. Measurements of Thermodynamic Properties for HFO-1123 and HFO-1123 + R32 Mixture. *15th International Refrigeration and Air Conditioning Conference at Purdue*, West Lafayette, IN, July 11-14, Paper 1688.

Huber, M.L., Friend, D.G., Ely, J.F., 1992. Prediction of the thermal conductivity of refrigerants and refrigerant mixtures. *Fluid Phase Equilibria*, 80: 249-261.

Hui, T. O., and J. R. Thome. 1985. A study of binary mixture boiling: boiling site density and subcooled heat transfer. *International Journal of Heat and Mass Transfer*, 28(5):919–928.

Jung, D., Radermacher, R., 1993, Prediction of evaporation heat transfer coefficient and pressure drop of refrigerant mixtures in horizontal tubes, *Int. J. Refrigeration*, vol. 16: p. 201-209.

Klein, S.A., McLinden, M.O. and Laesecke, A. (1997). An improved extended corresponding states method for estimation of viscosity of pure refrigerants and mixtures. *Int. J. Refrigeration* 20: 208-217.

Kondou, C., BaBa, D., Mishima, F., Koyama, S., 2013. Flow boiling of non-azeotropic mixture R32/R1234ze (E) in horizontal microfin tubes. *Int. J. Refrigeration* 36, 2366–2378.

Kondou, C., Mishima, F., Koyama, S., 2015. Condensation and evaporation of R32/R1234ze(E) and R744/R32/R1234ze(E) flow in horizontal microfin tubes. *Sci. Technol. Built Environ*. 21, 564–577.

Kondou, C., Matsuzono, T., Tsuyashima, T., Higashi, Y., 2018. Surface tension measurement of low GWP refrigerant mixture HFO-1123/HFC-32, *The 9th Asian Conference on Refrigeration and Air Conditioning ACRA2018*, June 11-13, 2018, Sapporo, Japan.

Kunz, O. and Wagner, W. The GERG-2008 Wide-Range Equation of State for Natural Gases and Other Mixtures: An Expansion of GERG-2004. *J. Chem. Eng. Data*, 57(11):3032-3091, 2012.

Lemmon, E.W., Huber, M.L., McLinden, M.O., 2013, Reference Fluid Thermodynamic and Transport Properties - REFPROP Ver. 9.1, National Institute of Standards and Technology, Boulder, CO, USA.

Mulero, A., and I. Cachadiña. 2014. Recommended Correlations for the Surface Tension of Several Fluids Included in the REFPROP Program. *Journal of Physical and Chemical Reference Data*, 43(2):023104.

Niederküger, M., Steiner, D., 1994, Flow boiling heat transfer to saturated pure components and non-azeotropic mixtures in a horizontal tube, *Chem. Eng. Prog.*, vol. 33: p. 261-275.

Silver, L. 1942. Gas cooling with aqueous condensation. *Trans. Institution of Chemical Engineers* 20(14):30–42.

Taylor, J.R. 1997. An Introduction to Error Analysis,2nd Ed.New York, NY: University Science Book; 73–7

Thome, J.R. 1983. Prediction of binary mixture boiling heat transfer coefficients using only phase equilibrium data. *International Journal of Heat and Mass Transfer* 26(7):965–74.

Thome, J.R., N. Kattan, and D. Favrat, 1997. Evaporation in microfin tubes: a generalized prediction model, Proc. Convective Flow and Pool Boiling Conf., Kloster Irsee, Germany, Paper VII-4.

Yonemoto, R., and S. Koyama. 2007. Experimental study on condensation of pure refrigerants in horizontal micro-fin tubes: Proposal of correlations for heat transfer coefficient and frictional pressure drop. *Trans. JSRAE* 24(2):139–48.

Yoshida, S., Mori, H, Kakimoto, Y., Ohishi, K., 2000. Dryout quality for refrigerants flowing in horizontal evaporator tubes. *Trans. JSRAE*, 4:511–20.

Nomenclature

d_{eq}	= equivalent inner diameter	(m)
d_o	= outer diameter	(m)
h	= enthalpy	(Jkg^{-1})
h_{fin}	= fin height	(m)
P	= pressure	(Pa)
q	= heat flux	(Wm^{-2})
Q	= heat transfer rate	(W)
T	= temperature	(°C)
V_{crit}	= critical molar volume	($cm^3\ mol^{-1}$)
X	= circulation mass fraction of liquid or bulk	(-)
$\bar{X}$	= mole fraction of liquid	(-)
x	= vapor quality	(-)
Y	= circulation mass fraction of vapor	(-)
$\Delta P/\Delta Z$	= effective heating length	($Pa\ m^{-1}$)
ΔZ	= effective heating length	(m)
α	= heat transfer coefficient	($Wm^{-2}K^{-1}$)
η_A	= enlargement ratio of heat transfer surface	(-)
λ	= thermal conductivity	($Wm^{-1}K^{-1}$)
$\bar{\theta}$	= surface fraction evaluated at liquid or bulk mole fraction	(-)
σ	= surface tension	($N\ m^{-1}$)

Subscripts

EOS = equation of state

H2O = water

R1123 = R1123

TS = test section

bottom = bottom

cal = calculated value

i = inlet

left = left

meas = measured value

o = outlet

r = refrigerant

right = right

sat = saturated state

top = top

tube = tube

wi = inner tube wall

wo = outer tube wall

Table 1 Instrumentation and measurement uncertainty.

Measured parameters	Instruments	Uncertainty
Refrigerant temp.	Sheathed K-type thermocouple, ϕ 1 mm	±0.05 °C
Refrigerant flow rate	Coriolis mass flow meter, Max. 50 kg h^{-1}	
Refrigerant absolute pressure	Strain gage type absolute pressure transducer, 5 MPa (for condensation test) 2 MPa (for evaporation test)	 ±10 kPa ±4 kPa
Refrigerant differential pressure	Strain gage type differential pressure transducer, 20 kPa (for condensation test) 50 kPa (for evaporation test)	 ±0.1 kPa ±0.2 kPa
Refrigerant composition	TCD gas-chromatography	±0.01 by mass
Tube wall temperature	T-type thermocouple, ϕ 0.127 mm	±0.05 °C
Water temperature	100 Ω Pt resistance thermometer, ϕ 2 mm	±0.03 °C
Water flow rate	Gear type volumetric flow meter, Max. 300 Lh^{-1}	±1.5 Lh^{-1}

Table 2 Dimensions of the test microfin tube.

	Outer diameter	Equivalent inner diameter, d_{eq}*	Wall thickness	Helix angle, β	Apex angle	Number of fins	Fin height	Area enlargement, η_A
	[mm]	[mm]	[mm]	[deg]	[deg]	[-]	[mm]	[-]
	6.03	5.21	0.324	18	15	30	0.269	2.62

* The diameter of an equivalent smooth tube envelops the same internal-free-flow-volume. That was obtained from the actual cross-sectional area A_{cross} and the helix angle β. $d_{eq} = \sqrt{(4A_{cross})/(\pi \cos\beta)}$

Table 3 Basic information and thermophysical properties of the tested refrigerants.

Average saturation temperature		at 40 °C		at 10 °C	
		R32	R1123/R32 (40/60 mass%)	R32	R1123/R32 (40/60 mass%)
ODP		0	0		
GWP		675	405		
ASHARE safety class		A2L	N/A* *flammability is expected as level 1		
Critical temperature	°C	78.15	69.05		
Saturation pressure[*1]	MPa	2.48	2.84	1.11	1.31
Temperature glide[*1]	K	-	0.64	-	1.10
Density (vapor)[*1]	kg m^{-3}	73.3	105.8	30.2	43.1
Density (liquid)[*1]		893	891	1020	1036
Latent heat[*1]	kJ kg^{-1}	237	175	299	236
Surface tension[*2]	mN m^{-1}	4.489	3.60	9.26	8.27
Viscosity (liquid)[*3]	μPa s	95.0	88.2	134.6	126.3
Thermal conductivity (liquid)[*3]	mW $m^{-1}K^{-1}$	115	92.7	137	113

*1 - calculated using REFPROP9.1 KW0 default model with R1123 EOS of Higashi and Akasaka (2016)

*2 - calculated using the empirical correlation of Kondou et al. (2018)

*3 - estimated using the ECS model provided by REFPROP9.1 (Klein et al., 1997; Huber et al., 1992)

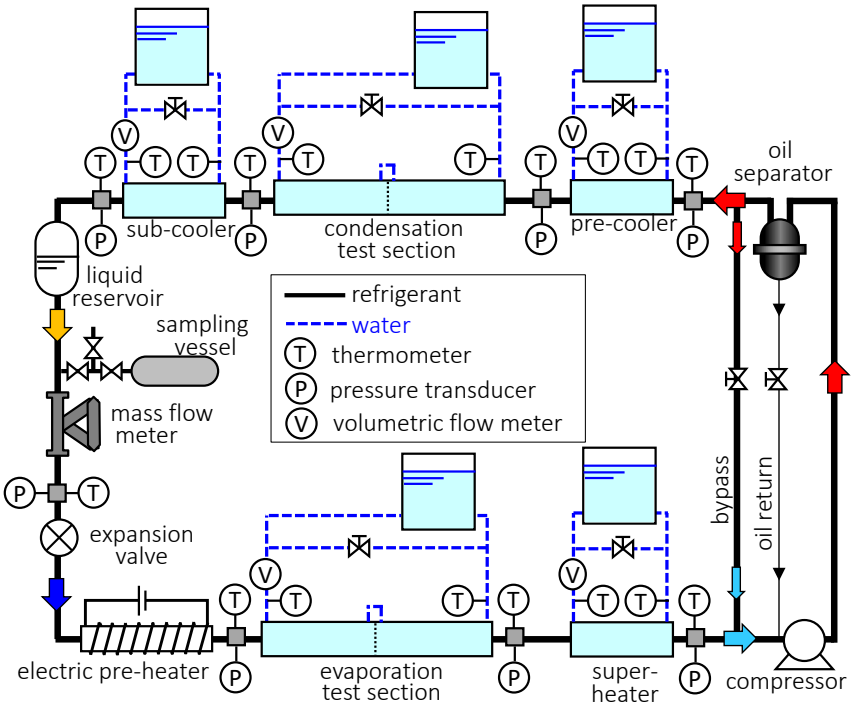

(a) test loop

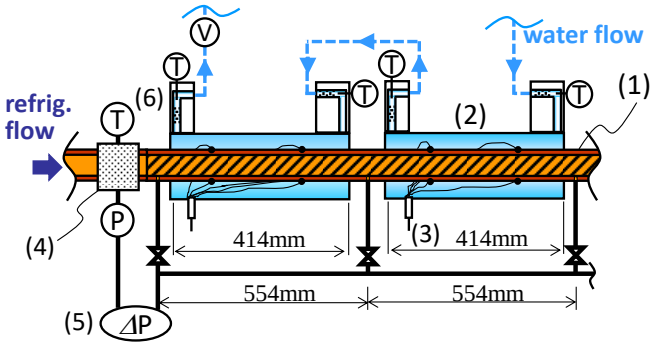

(1) test microfin tube
(2) water jacket
(3) thermocouples
(4) mixing chamber for refrigerant
(5) differential pressure transducer
(6) mixing chamber for water

(b) structure of the test section (evaporator)

Fig. 1 Experimental apparatus

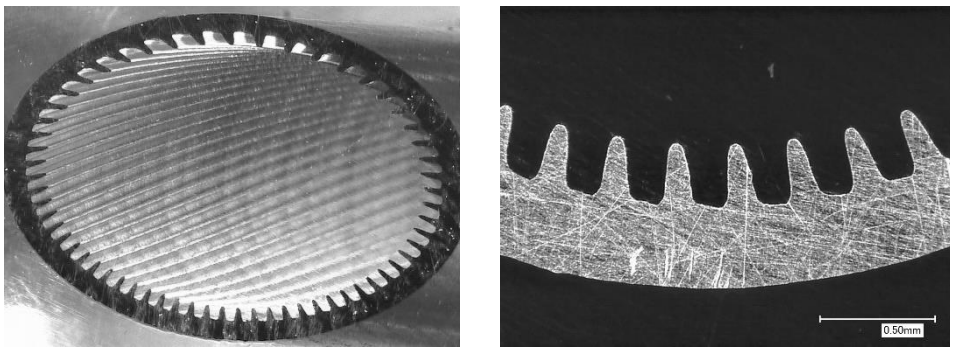

Fig. 2 Sectional view of the tested microfin tube

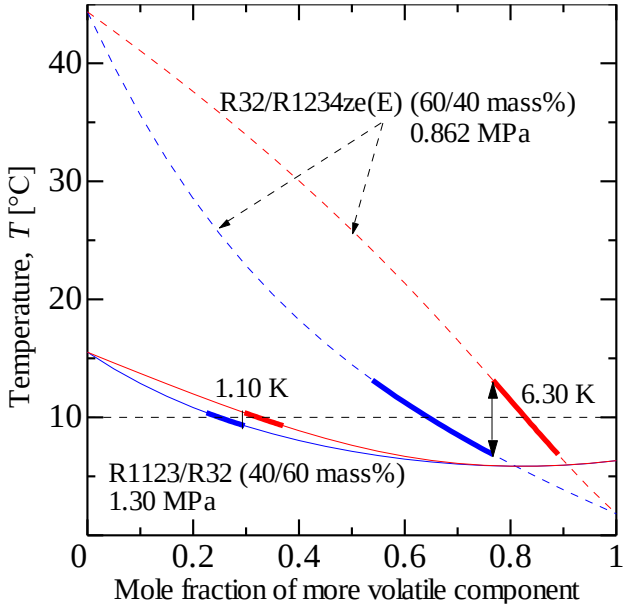

Fig. 3 Phase equilibria of R1123/R32 and other R410A alternative candidate R32/R1234ze(E) at an average saturation temperature of 10 °C.

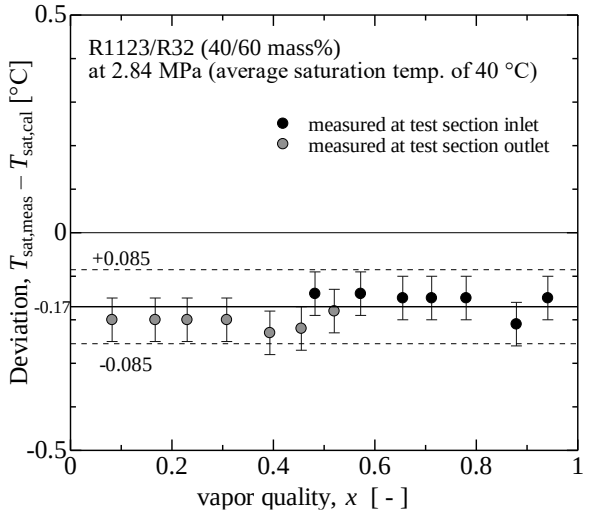

(a) for condensation test

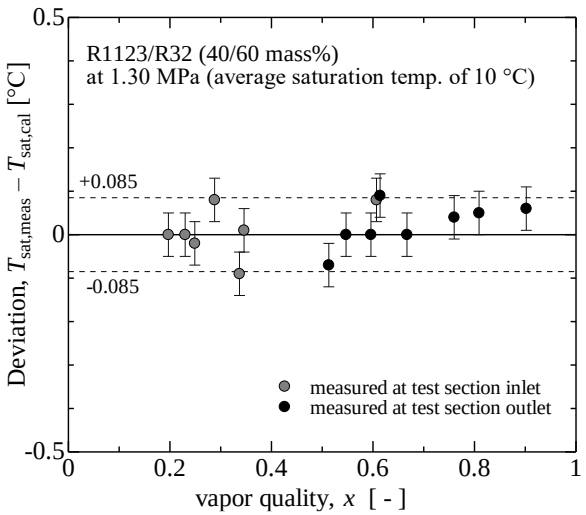

(b) for evaporation test

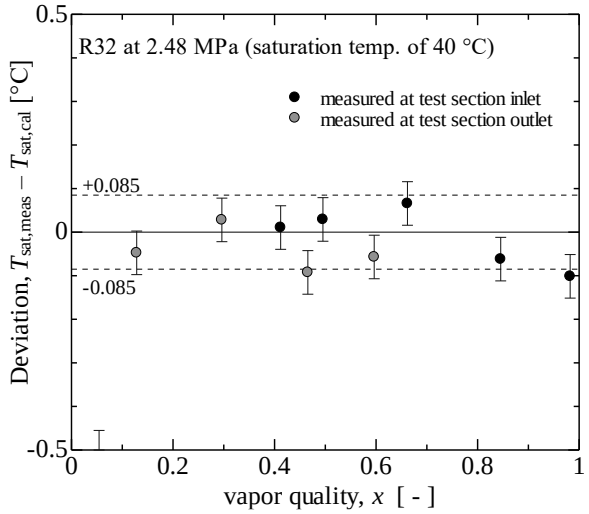

(c) for condensation test

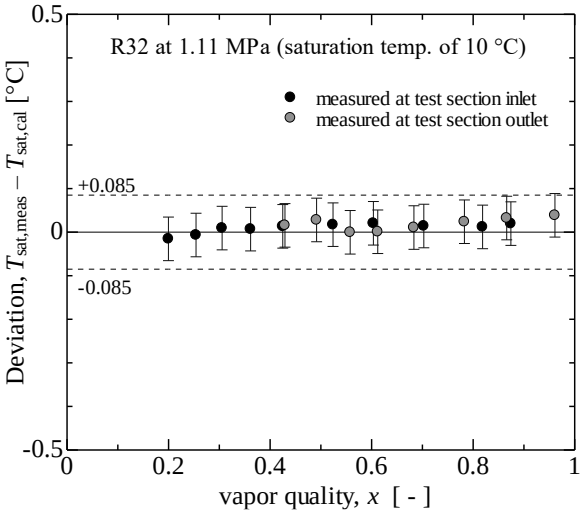

(d) for evaporation test

Fig. 4 Comparison on refrigerant saturation temperature between the measured and calculated with KW0 model.

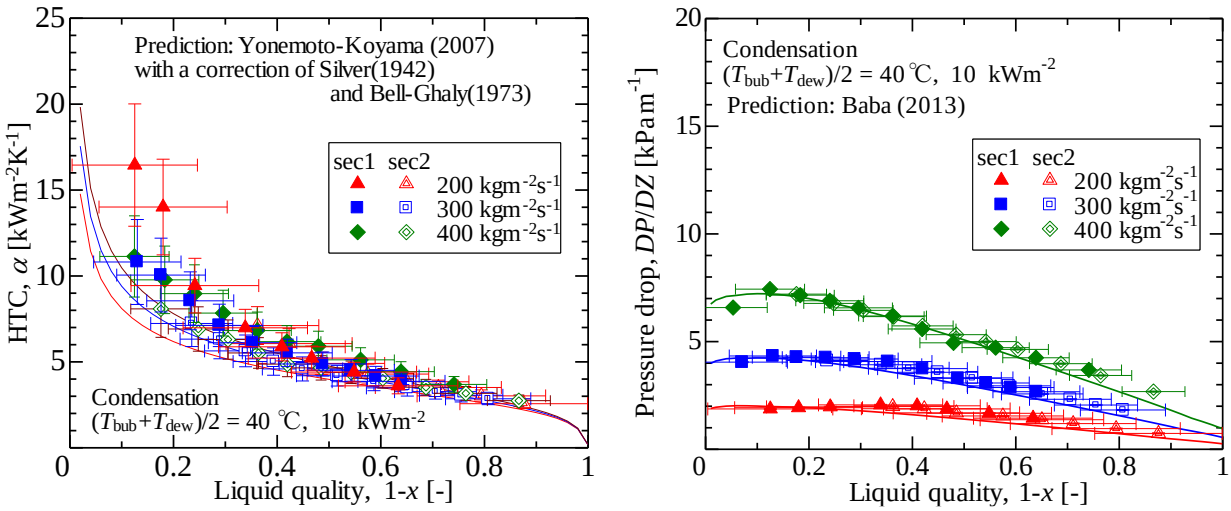

(a) heat transfer coefficient (b) pressure drop

Fig. 5 R1123/R32 (40/60 mass%) condensation test results at various mass velocities.

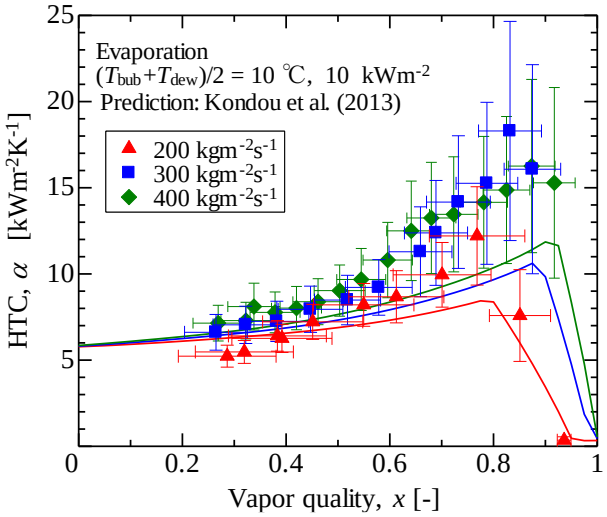

(a) heat transfer coefficient at various mass velocities

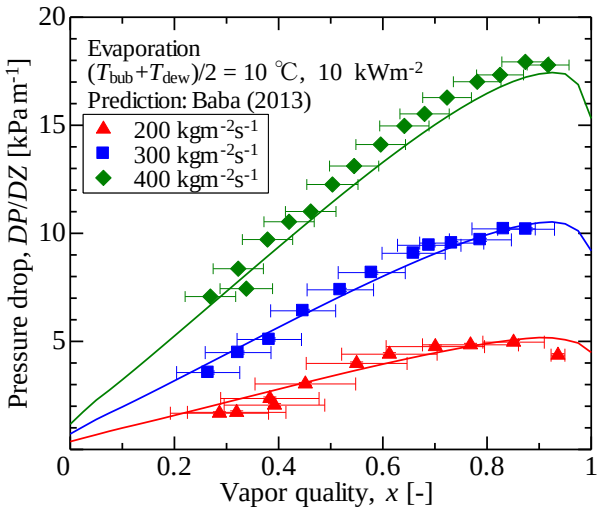

(b) pressure drop at various mass velocities

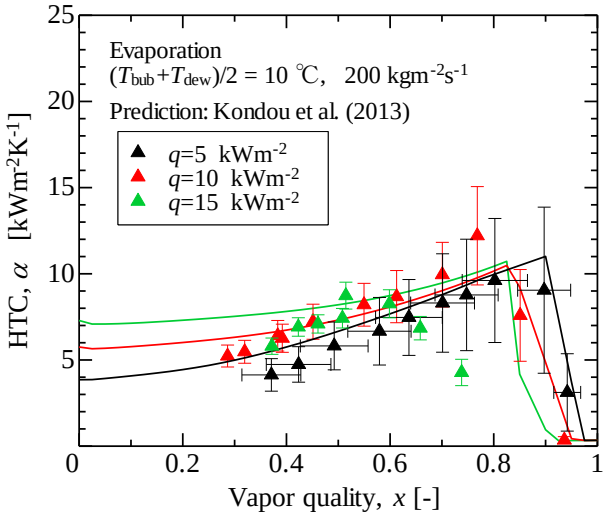

(c) heat transfer coefficient at various heat fluxes

Fig. 6 R1123/R32 (40/60 mass%) evaporation test results at various mass velocities and heat fluxes.

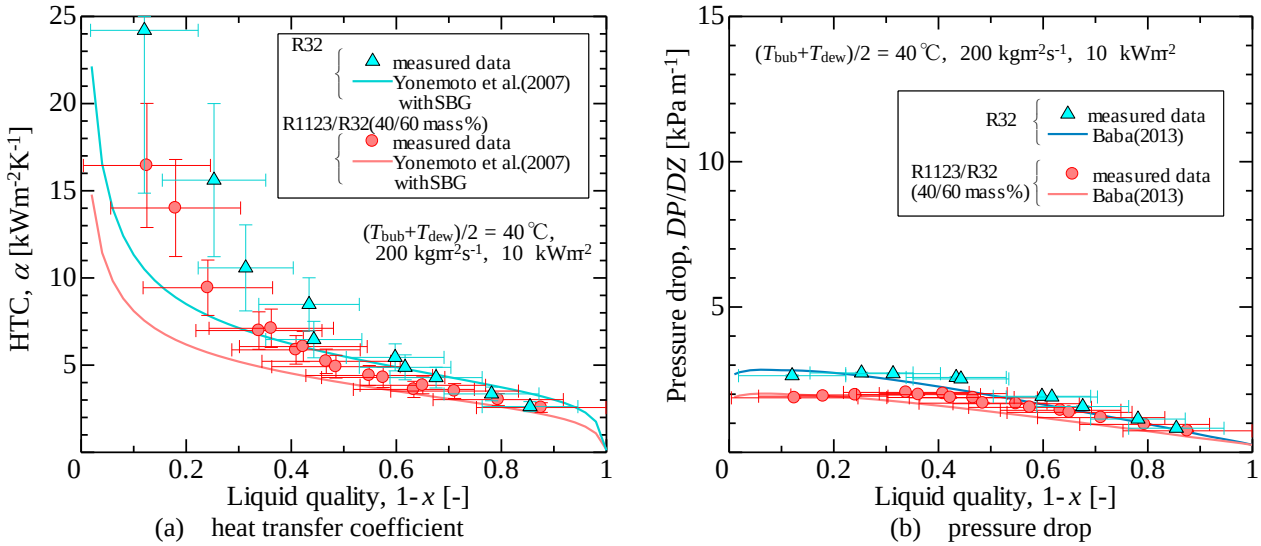

(a) heat transfer coefficient (b) pressure drop

Fig. 7 Comparison between R1123/R32(40/60 mass%) and R32 at 40 °C during condensation

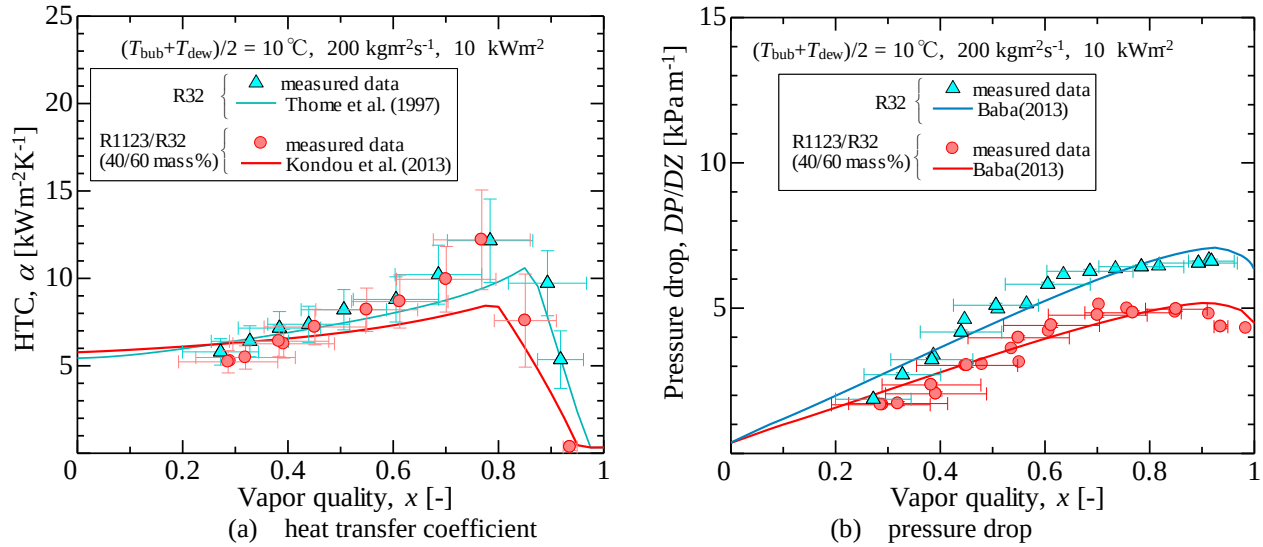

(a) heat transfer coefficient (b) pressure drop

Fig. 8 Comparison between R1123/R32(40/60 mass%) and R32 at 10 °C during evaporation

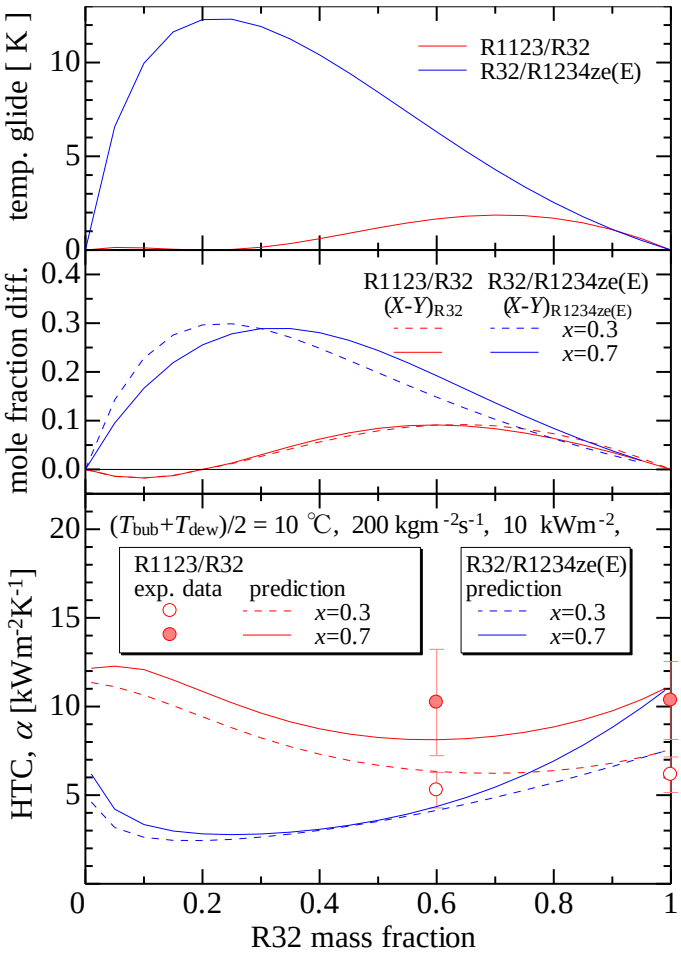

Fig. 9 Estimated change in HTC of binary mixtures against R32 mass fraction.